Highly Deformed Structures in the Mass~130 Region and Their Relative Quadrupole Moments

F.G. Kondev†, M.A. Riley†, E.S. Paul‡, T.B. Brown†[1], R.M. Clark¶, M. Devlin§, P. Fallon¶, D.J. Hartley†[2], I.M. Hibbert‖[3], D.T. Joss‡, D.R. LaFosse§[4], R.W. Laird†, F. Lerma§, M. Lively†, P.J. Nolan‡, N.J. O'Brien‖, J. Pfohl†, D.G. Sarantites§, R.K. Sheline†, S.L. Shepherd‡, J. Simpson+ and R. Wadsworth‖

† *Department of Physics, Florida State University, Tallahassee, Florida 32306*
‡ *Oliver Lodge Laboratory, University of Liverpool, Liverpool L69 7ZE, United Kingdom*
¶ *Nuclear Science Division, Lawrence Berkeley Laboratory, Berkeley, California 94720*
§ *Department of Chemistry, Washington University, St. Louis, Missouri 63130*
‖ *Department of Physics, University of York, York Y01 5DD, United Kingdom*
+ *CLRC, Daresbury Laboratory, Daresbury, Warrington, WA4 4AD, United Kingdom*

Abstract. The quadrupole moments for variety of configurations, involving the $9/2^+[404]$ ($g_{9/2}$) proton, $1/2^+[660]$($i_{13/2}$) and $1/2^-[541]$ ($f_{7/2}$,$h_{9/2}$) neutron orbitals, were measured using the Doppler-shift attenuation method in a wide range of nuclei in the mass~130 region. While the involvement of the first two orbitals leads to quadrupole deformations that are comparable to those observed for the so-called superdeformed bands in this mass region, the β_2 values for structures that include the $1/2^-[541]$ neutron are found to lie intermediate between those observed for normally deformed and highly deformed bands.

INTRODUCTION

The recent studies of highly deformed (β_2=0.3–0.4), sometimes referred to as "superdeformed", structures in the region near mass~130 have revealed an important interplay between microscopic shell effects, such as the occurrence of large gaps in the nucleon single-particle energies, and the occupation of high-j low-Ω (intruder) orbitals in driving the nucleus towards higher deformation. Initially, it was thought that only the involvement of one or more $i_{13/2}$ neutrons could result in a strong polarization on the nuclear shape in this mass region [1]. However, it was recently shown that certain strongly coupled bands, built upon the $9/2^+[404]$ ($g_{9/2}$) proton orbital in the odd-Z ^{131}Pr [2] and ^{133}Pm [3] isotopes, exhibit quadrupole deformations comparable to the values found for highly deformed structures which include $i_{13/2}$ neutrons. Furthermore, for nuclei below $N = 73$ where the occupancy of the $\nu i_{13/2}$ orbital is energetically unfavored, there are indications that bands involving the $1/2^-[541]$ ($f_{7/2}$,$h_{9/2}$) neutron may also be highly deformed [4,5].

In order to provide further experimental evidence about the highly deformed character of these structures, as well as to elucidate the impact of the occupation of specific orbitals along with the "core stabilization" effect from the shell gaps on deformation, accurate lifetime measurements for a large number of bands have been measured. While the quadrupole moment, Q_0, for some of these bands were measured in the past using the Doppler-shift attenuation method (DSAM), conclusive comparisons were limited owing to systematic distinctions between experimental setups such as varying reactions and target retardation properties. Specifically, due to differences in the parameterization of the nuclear and electronic stopping powers, which act as an "internal clock" in the DSAM lifetime measurements, large variations in the measured Q_0 values are reported for the

---

[1] Present address: Chemistry Department, University of Kentucky, Lexington, Kentucky 40506.
[2] Present address: Department of Physics and Astronomy, University of Tennessee, Knoxville, Tennessee 37996.
[3] Present address: Oliver Lodge Laboratory, University of Liverpool, Liverpool L69 7ZE, United Kingdom.
[4] Present address: Department of Physics and Astronomy, SUNY at Stony Brook, New York 11794.

CP481, *Nuclear Structure 98*, edited by C. Baktash

same band by different authors. The absence of adequate experimental information on the time structure of the quasicontinium sidefeeding contributions also results in an additional inaccuracy on the measured quadrupole moments. In the current work we have greatly reduced these systematic problems by measuring the lifetime decay properties of a large selection of bands in different nuclei under nearly identical experimental conditions in terms of angular momentum input, excitation energy and recoil velocity profile. Furthermore, by exploiting the high efficiency and resolving power of the modern γ-ray detector arrays it was possible, in cases of favorable statistics, to greatly minimize the effect of sidefeeding on the measured quadrupole deformations, by gating on shifted transitions at the top of the band of interest, thus gaining some insight into the nature and time scale of the sidefeeding.

EXPERIMENTAL CONDITIONS AND DATA REDUCTION

High-spin states in a wide range ($Z = 58-61$) of nuclei were populated after fusion of a ^{35}Cl beam with ^{105}Pd target nuclei. Thin and backed target experiments were performed at the 88-Inch Cyclotron at the Lawrence Berkeley National Laboratory with beam energies of 180 (thin target) and 173 MeV (backed target). The thin target consisted of an isotopically enriched ^{105}Pd foil with a thickness of 500 μg/cm^2. The backed target was a 1 mg/cm^2 thick ^{105}Pd foil mounted on a 17 mg/cm^2 Au backing. Emitted γ-rays were collected using the GAMMASPHERE spectrometer [6] consisting of 57 (thin target) and 97 (backed target) HPGe detectors arranged in seventeen rings located at θ=17.3°, 31.7°, 37.4°, 50.1°, 58.3°, 69.8°, 79.2°, 80.7°, 90.0°, 99.3°, 100.8°, 110.2°, 121.7°, 129.9°, 142.6°, 148.3° and 162.7°. The evaporated charged particles were identified with the MICROBALL detector system [7], whose selection capabilities allowed a clean separation of the different charged particle channels. The present work focuses on the properties of structures which involve the important $9/2^+[404]$ ($g_{9/2}$) proton, $1/2^+[660](i_{13/2})$ and $1/2^-[541]$ ($f_{7/2}$,$h_{9/2}$) neutron orbitals, in the odd-N (Z=60) ^{133}Nd (populated in the αp2n channel) and ^{135}Nd (3p2n) isotopes, and the odd-Z (Z=59) ^{130}Pr (2α2n), ^{131}Pr (2α1n) and ^{132}Pr (1α2p2n) nuclei. Typically more than about 50×10^6 (thin target) and 20×10^6 (backed target) events (of a fold $\geq$3) per particle gated channel were collected.

In the off-line analysis, the thin target data were unfolded into γ^3 coincidences and incremented into three-dimensional cubes. Background subtracted, doubly-gated spectra were then produced for each particular cascade and were examined in order to construct the level schemes. Non-symmetrical (31.7° and 37.4° vs. 90°) matrices were also constructed which enabled γ-ray multipolarities to be deduced using the method of directional correlation from oriented states (DCO).

The backed target data were used to extract the quadrupole deformation using the centroid-shift technique in conjunction with the Doppler-shift attenuation method [8]. This was done in two ways. In the first method, the data were sorted into two-dimensional matrices in which one axis consisted of "forward" (31.7° and 37.4°) or "backward" (142.6° and 148.3°) group of detectors and the other axis was any coincident detector. Spectra were generated by summing gates on the cleanest, fully stopped transitions at the bottom of the band of interest and projecting the events onto the "forward" and "backward" axes. These spectra were then used to extract the fraction of the full Doppler shift, F(τ), for transitions within the band of interest. The use of this approach allowed the sidefeeding contributions to take full effect when the Q_0 values are deduced, since the measured F(τ) values depend not only on the lifetime of a particular state, but also on the time history of all levels within cascades which precede it. In the second method, the data were sorted into a number of double-gated spectra which contained counts registered by particular group of detectors. Specifically, for the relatively strongly populated $\nu i_{13/2}$ bands in ^{133}Nd and ^{135}Nd, gates were also set on in-band "moving" transitions (i.e., those which showed Doppler shift) in any ring of detectors and data were incremented into separate spectra for events detected at "forward", "90°" and "backward" angles. Since the gating transitions are Doppler-shifted, ring-by-ring energy-dependent Doppler corrections were applied in the sorting procedure using the formula:

$$C = C_0(1 + F(\tau)\beta_0 \cos\theta) \quad (1)$$

where C_0 and C are the gain matched raw and Doppler-corrected channel numbers, respectively, and β_0 refers to the initial velocity of the recoiling nucleus. The F(τ) values for transitions within the band of interest were calculated (see below in the text) iteratively by varying the in-band Q_0 until the Doppler-corrected peak centroids were perfectly matched in all detector rings. This allowed the correct coincidence relationships to be achieved in the gating procedure. Consequently, non-Doppler corrected spectra were written on disk and were used to extract the final F(τ) values. Examples of resulting spectra, after background subtraction, for

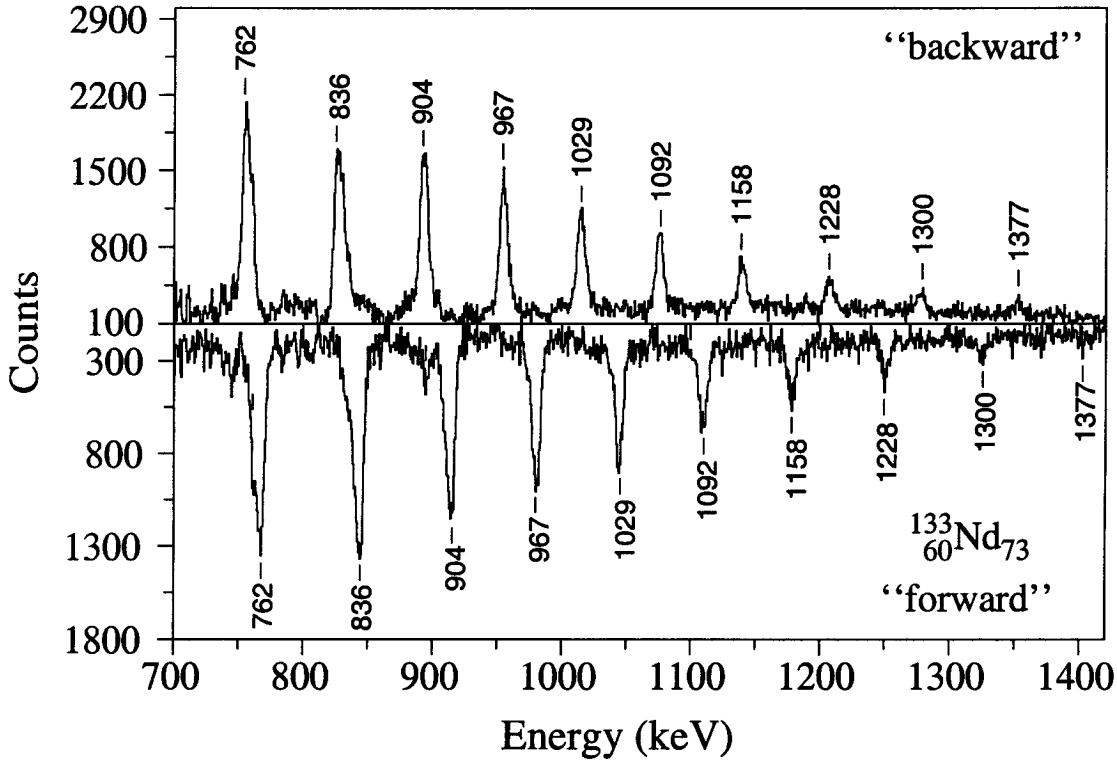

FIGURE 1. Coincidence γ-ray spectra for the $1/2^+[660]$ ($i_{13/2}$) band in ^{133}Nd formed from combinations of all double gates on in-band transitions from 345 keV up to 1228 keV. The peaks are labeled with the unshifted energies.

the $\nu 1/2^+[660]$ ($i_{13/2}$) band in ^{133}Nd are shown in fig. 1. It should be noted, that the implementation of this method made it possible to eliminate the effect of sidefeeding for states lower in the cascade, i.e. for those below the levels depopulated by the gating transitions.

In the off-line analysis various programs from the RADWARE interactive package [9] were employed.

EXPERIMENTAL RESULTS AND DISCUSSION

In order to extract the intrinsic quadrupole moments from the experimental $F(\tau)$ values, calculations using the code FITFTAU [10] were performed. The $F(\tau)$ curves were generated under the assumption that the band has a constant Q_0 value. In the modeling of the slowing process of the recoiling nuclei, the stopping powers were calculated using the 1995 version of the code TRIM [11] which uses the most recent evaluation of existing data. The corrections for multiple scattering were introduced using the prescription given by Blaugrund [12]. Where appropriate, the sidefeeding into each state was taken into account according to the experimental in-band intensity profile using a rotational cascade of three transitions with the same Q_0 as the in-band states. The impact of the number of sidefeeding cascades on Q_0 was investigated and found to be much smaller than the statistical uncertainties. Table 1 summarizes the measured Q_0 values and the corresponding quadrupole deformations, β_2. It should be emphasized, that although the uncertainties in the stopping powers and the modeling of the sidefeeding may contribute an additional systematic error of 15–20% in the absolute Q_0 values, the relative deformations are considered to be accurate to a level of 5–10% since the bands were studied under nearly identical conditions. Such precision allowed a clear differentiation in the Q_0 values to be made, which was used in turn as evidence for the involvement of specific orbitals within a band configuration.

TABLE 1. Quadrupole moments and deformations for selected bands.

Nucleus	Configuration [a]	Q_0, eb [β_2] [b] Present	Previous	Reference
^{133}Nd	$\nu i_{13/2}$	5.8(4) [0.32(3)]	6.0(7) [0.33(3)]	[13]
		6.4(4) [0.36(3)] [c]	6.7(7)[0.37(4)] [d]	[13]
			7.4(7)[0.41(3)] [e]	[14]
^{135}Nd	$\nu i_{13/2}$	5.1(5) [0.28(3)]	5.4(10) [0.30(5)]	[15]
		5.5(6) [0.30(4)] [c]	7.4(10) [0.40(5)] [f]	[15]
			7.3(10) [0.37(5)] [g]	[16]
^{130}Pr	$\pi g_{9/2} \otimes \nu h_{11/2}$	6.1(4) [0.35(2)]		
^{131}Pr	$\pi g_{9/2}$	5.3(4) [0.31(2)]	5.5(8) [0.32(5)]	[2]
^{130}Pr	$\pi h_{11/2} \otimes \nu(f_{7/2},h_{9/2})$ (band 1)	4.3(3) [0.25(2)]		
	$\pi h_{11/2} \otimes \nu(f_{7/2},h_{9/2})$ (band 2)	4.5(3) [0.26(2)]		
^{132}Pr	$\pi h_{11/2} \otimes \nu(f_{7/2},h_{9/2})$	4.1(3) [0.24(1)]		
^{130}Pr	$\pi h_{11/2} \otimes \nu d_{5/2}$	3.4(2) [0.20(1)]		
^{131}Pr	$\pi h_{11/2}$	3.3(2) [0.19(1)]	3.9(3) [0.23(2)]	[2]

[a] $\pi g_{9/2}$: $9/2^+[404]$, $\pi h_{11/2}$: $3/2^-[541]$, $\nu h_{11/2}$: $7/2^-[523]$, $\nu d_{5/2}$: $5/2^+[402]$, $\nu(f_{7/2},h_{9/2})$: $1/2^-[541]$, $\nu i_{13/2}$: $1/2^+[660]$.

[b] Deduced using the centroid-shift technique with sidefeeding quadrupole moment, Q_{0sf} equal to Q_0.

[c] Deduced by gating above the level of interest (see the text for details).

[d] Deduced using the lineshape technique with Q_{0sf}=5.3 eb.

[e] Deduced using the lineshape technique with sidefeeding time distributions about 1.4 times slower than the in-band lifetimes.

[f] Deduced using the lineshape technique with Q_{0sf}=3.5 eb.

[g] Deduced using the centroid-shift technique with Q_{0sf}=3.0(5) eb. Note that although nearly identical Q_0 values were measured in ref. [15,16] the quoted β_2 values differ by ~7%.

Bands involving the $1/2^+[660]$ ($i_{13/2}$) neutron orbital

Collective structures built upon the $1/2^+[660]$ ($i_{13/2}$) intruder neuton orbital have been observed in the chain of odd-N (Z=60) Nd isotopes from ^{133}Nd up to ^{137}Nd [17,18]. These bands were connected to the normally deformed structures [18–23], so that their spin, parity and excitation energy are unambiguously determined. In addition, the g-factor experiment performed in the case of ^{133}Nd [14] independently confirms the $\nu 1/2^+[660]$ configuration assignment. Quadrupole moment measurements were carried out previously using both the centroid-shift and lineshape DSAM techniques [13–16,24]. Lifetimes of low-spin members of the band in ^{135}Nd were also measured via the Doppler-shift recoil-distance method [25]. The $F(\tau)$ values and the corresponding quadrupole deformations deduced in the current work when gates were set on the stopped 409, 440, 513 and 603 keV transitions in ^{133}Nd, and 546 and 676 keV γ-rays in ^{135}Nd are shown in Figs. 2c and 2d. Our observations are in agreement with the previously measured quadrupole deformations for the band in ^{133}Nd [13], as well as with the centroid-shift results for the structure in ^{135}Nd reported by Diamond *et al.* [15]. Importantly, they clearly indicate that the band in ^{133}Nd is more deformed than that in ^{135}Nd. The comparison of the intensity profiles for those two bands, shown in Figs. 2a and 2b, reveals that the sequence in ^{135}Nd is fed more from the side over a range of transitions for which the $F(\tau)$ values change very rapidly. Such a behavior led to speculations that the sidefeeding lifetimes could be much slower when compared to that for the in-band levels. In fact, the lineshape analysis of Diamond *et al.* [15], as well as recent centroid-shift observations by Petrache *et al.* [16], suggested that the sidefeeding lifetimes were about factor of four slower, thus leading to a quadrupole deformation that exceeded the value in ^{133}Nd (see Table 1). Figures 2e and 2f show our observations, when spectra gated on the Doppler-shifted in-band 1029, 1092, 1158, 1228 and 1300 keV γ-rays in ^{133}Nd, and 947, 1012, 1078, 1146, and 1216 keV γ-rays in ^{135}Nd, were used. We found a roughly 10% increase in the deformation of both these two bands, compared to values deduced when gates were set on stopped transitions. We estimated that the sidefeeding lifetimes are only about 1.3–1.4 times slower than those

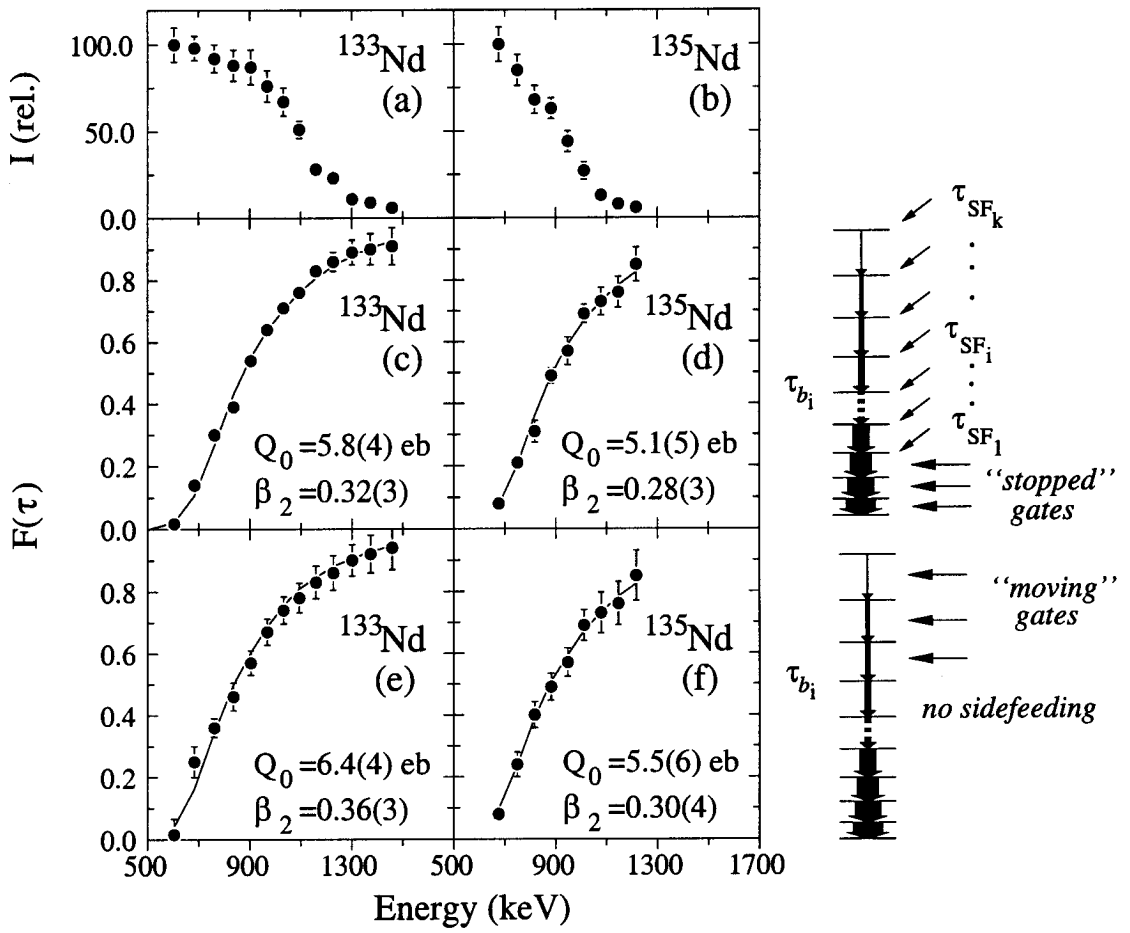

FIGURE 2. Intensity profiles (a) and (b), F(τ) values and corresponding quadrupole deformations deduced by gating on stopped transitions (c) and (d), and "moving" transitions (e) and (f) for the $1/2^+[660]$ ($i_{13/2}$) bands in ^{133}Nd and ^{135}Nd, respectively.

for the in-band levels. Similar results for the ratio of in-band to sidefeeding lifetimes were recently reported by Clark *et al.* [26] in studying the relative deformations of structures which include one or two $\nu i_{13/2}$ orbitals in the neighboring ^{131}Ce and ^{132}Ce isotopes.

The present observations, together with the values for the band in ^{137}Nd (Q_0=4.0(5) [β_2=0.22(3)]) [13], indicate that in the odd-N Nd nuclei there is a systematic decrease in the deformation of the $\nu i_{13/2}$ band as the neutron number increases. Similar behavior, for the same configuration, was also observed in the neighboring ^{135}Sm (N=73) and ^{137}Sm (N=75) isotopes [27]. Such a trend was predicted previously by Total Routhian Surface and Ultimate Cranker calculations with pairing [13,21], as well as by Cranked Nilsson-Strutinsky calculations [28] which do not include pairing. The excitation energy as a function of spin for the $\nu i_{13/2}$ bands in ^{133}Nd (N=73), ^{135}Nd (N=75) and ^{137}Nd (N=77) are shown in Fig. 3a. As can be seen, the band in ^{133}Nd is lower in energy compared to those in ^{135}Nd (ΔE$\sim$0.6 MeV) and ^{137}Nd (ΔE$\sim$1.6 MeV), thus implying that the neutron Fermi level is located closer to the $1/2^+[660]$ Nilsson configuration at $N = 73$. As a consequence of the rapid downslope of this orbital with increasing the deformation, the higher excitation energy of the bands in ^{135}Nd and ^{137}Nd supports the experimental observations that they are less deformed, as illustrated in Fig. 3b.

Another interesting feature is the extra deformation for the $\nu i_{13/2}$ band in Z=58 ^{131}Ce (Q_0=7.4(3) *e*b [β_2=0.43(1)]) [26] compared to the values measured for the same configuration in the Z=60 ^{133}Nd and Z=62 ^{135}Sm (Q_0=7.0(7) *e*b [β_2=0.37(4)]) [27] isotones ($N = 73$). The presence of two proton "holes" in the upsloping $g_{9/2}$ proton orbital at Z=58 (Ce) and their absence in the Nd and Sm isotopes is suggested [28] to result in an additional enhancement of the deformation in the Ce nuclei. By comparing the relative deformations within

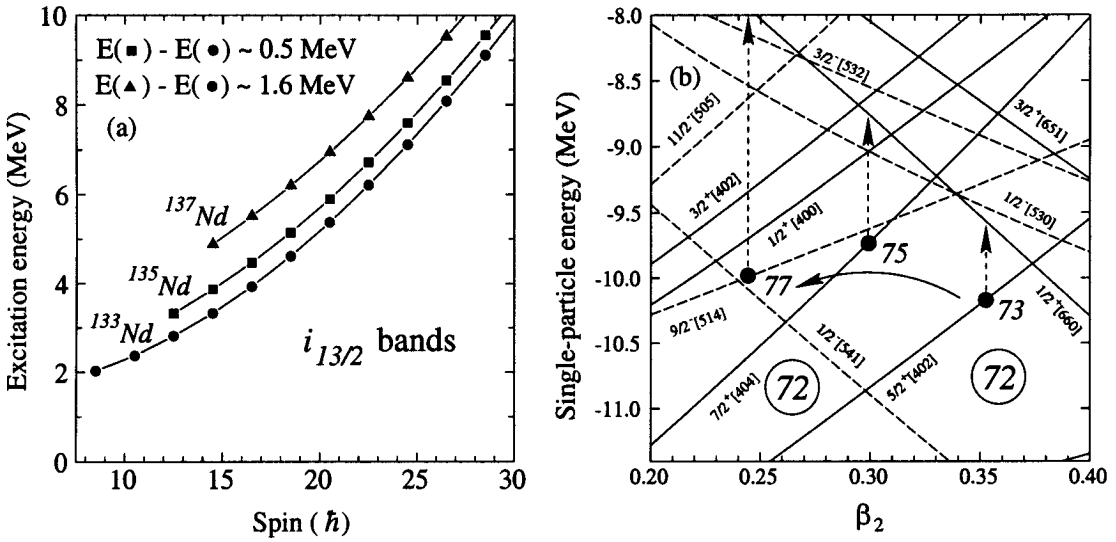

FIGURE 3. (a) Excitation energy as a function of spin for the $1/2^+[660]$ ($i_{13/2}$) bands in ^{133}Nd ($N = 73$), ^{135}Nd ($N = 75$) and ^{137}Nd ($N = 77$). (b) Neutron single-particle levels as a function of quadrupole deformation (γ=0°, β_4=0) calculated using the Woods-Saxon potential.

the $N = 73$ isotones the contribution of the partial occupation of the $\pi g_{9/2}$ orbital can be deduced as:

$$\delta\beta_2 = \beta_2(^{131}Ce) - \beta_2(^{133}Nd) = 0.43(1) - 0.36(3) = 0.7(4) \tag{2}$$

$$\delta\beta_2 = \beta_2(^{131}Ce) - \beta_2(^{135}Sm) = 0.43(1) - 0.37(4) = 0.6(5) \tag{3}$$

Thus, taking the measured quadrupole deformations for the bands in ^{135}Nd and ^{137}Nd as a base, then one may expect Q_0~6.5 and 5.1 *e*b for the $\nu i_{13/2}$ structures in ^{133}Ce and ^{135}Ce, respectively, which are not yet measured.

Bands involving the $9/2^+[404]$ ($g_{9/2}$) proton orbital

Initially, a band built upon the $9/2^+[404]$ ($g_{9/2}$) proton orbital was observed in ^{131}Pr by Galindo-Uribarri *et al.* [2]. This work has established a value of Q_0=5.5(8) *e*b [β_2=0.32(5)] for this band which is much larger than Q_0=3.9(3) *e*b [β_2=0.23(2)] deduced for the normally deformed $\pi 3/2^-[541]$ ($h_{11/2}$) structure in the same nucleus. Recently, Brown *et al.* [29] have observed a strongly coupled band in the neighboring odd-odd ^{130}Pr isotope which was suggested to include the $9/2^+[404]$ ($g_{9/2}$) proton orbital coupled to the $7/2^-[523]$ ($h_{11/2}$) neutron. The measured and calculated $F(\tau)$ values for this structure, as well as those for the normally deformed $\pi 3/2^-[541]$ ($h_{11/2}$)$\otimes\nu 5/2^+[402]$ ($d_{5/2}$) band are shown in Fig. 4a. The results for the $\pi g_{9/2}$ and $\pi h_{11/2}$ configurations in ^{131}Pr, deduced from the current work, are presented in Fig. 4b. We report Q_0=6.1(5) *e*b [β_2=0.35(3)] for the $\pi g_{9/2}\otimes\nu h_{11/2}$ band [30], which is similar or perhaps slightly larger compared to the value for the $\pi g_{9/2}$ band in ^{131}Pr. Our observations for the quadrupole deformations of the $\pi g_{9/2}$ and $\pi h_{11/2}$ bands in ^{131}Pr are in agreement with the values reported by Galindo-Uribarri *et al.* [2]. The new results for the highly deformed band in ^{130}Pr is the first direct experimental confirmation of the deformation-driving character of the $\pi g_{9/2}$ orbital in an odd-odd nucleus in the mass~130 region. It is notable that the deformation of structures that involve the $\pi 9/2^+[404]$ ($g_{9/2}$) configuration is comparable to those for the $1/2^+[660]$ ($i_{13/2}$) bands in the neighboring nuclei ^{133}Nd and ^{135}Nd isotopes (see Table 1), thus confirming the important role played by the former orbital in building highly deformed structures in the region.

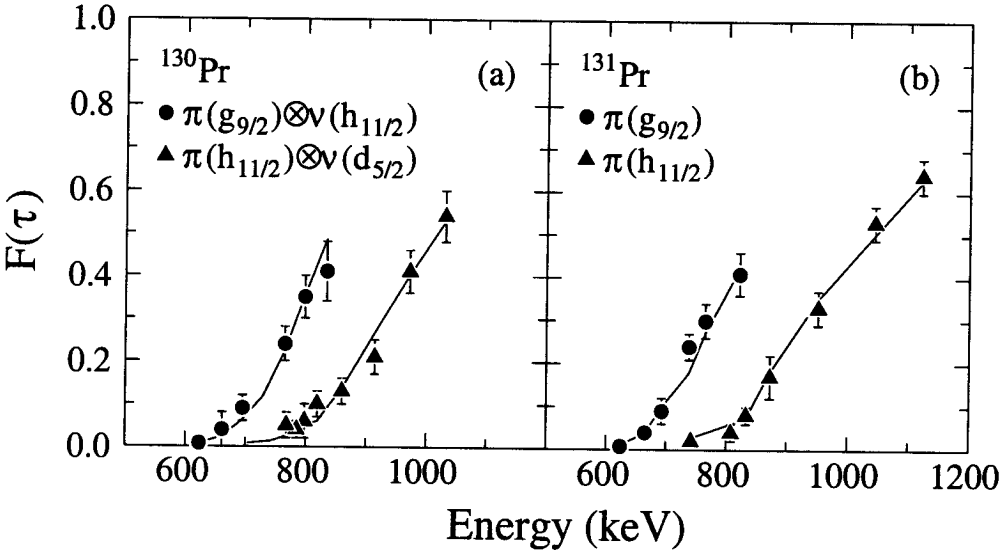

FIGURE 4. The experimental and calculated F(τ) values as a function of γ-ray energy for selected bands in ^{130}Pr and ^{131}Pr. Calculated curves as shown as solid lines and correspond to the best fit to the data.

Bands involving the 1/2$^-$[541] ($f_{7/2}$,$h_{9/2}$) neutron orbital

Two decoupled bands, referred to as band 1 and band 2 in the current work, were identified in ^{130}Pr in agreement with the parallel work of Smith *et al.* [31]. We confirm the previously reported decoupled band in ^{132}Pr [32,33], but we propose different spin values compared to the work of Shi *et al.* [33] (note that no spin assignments were given by Hauschild *et al.* [32]), and identify several additional in-band and inter-band transitions. Sample γ-ray coincidence spectra for all three bands from the thin target experiment are shown in Figs. 5a, 5b and 5c.

The band in ^{132}Pr decays via several branches to the yrast $\pi h_{11/2}\otimes\nu h_{11/2}$ structure [33,34] which enabled firm spin and parity (relative to the $\pi h_{11/2}\otimes\nu h_{11/2}$ structure) to be assigned. For example, the DCO ratio of 0.66(6), deduced for the 576.5 keV inter-band transition which feeds the 10$^+$ level of the $\pi h_{11/2}\otimes\nu h_{11/2}$ band [34], using the 541.3 keV stretched quadrupole transition as a gate, implies that the former γ-ray has a dipole character. Note, that a DCO ratio of approximately unity is expected for a ΔI=2 transition under the same gating condition. The unstretched I$\rightarrow$I assignment for the 576.5 keV γ-ray can be excluded given the relative population of these structures, thus suggesting odd spins for the decoupled band. The observation of the 707.5 keV γ-ray to the 9$^+$ state of the $\pi h_{11/2}\otimes\nu h_{11/2}$ band in parallel with the 576.5 keV transition and the measured intensity ratio of $I_\gamma(708)/I_\gamma(577)$=0.30(4) (see also Fig. 1) indicate that the former transition is a stretched quadrupole, thus establishing positive parity for the band. Band 1 in ^{130}Pr is also observed to decay to levels of the $\pi h_{11/2}\otimes\nu h_{11/2}$ band [34,35], in a way similar to that revealed for the decoupled structure in ^{132}Pr, and is also assigned odd spins and positive parity. The decay path of the second band in ^{130}Pr was difficult to establish, however, it was clear that it proceeded through level(s) at the bottom of the $\pi h_{11/2}\otimes\nu h_{11/2}$ band [34,35], as well (see Fig. 5b). The positive parity and even spins are tentatively assigned to this band. These observations, together with the measured rotational alignments, band crossing properties and the orbitals expected near both the proton and neutron Fermi surfaces, led us to conclude that the configuration of the decoupled structures includes the 1/2$^-$[541] ($f_{7/2}$,$h_{9/2}$) neutron orbital coupled to the 3/2$^-$[541] ($h_{11/2}$) proton. Such an interpretation is also supported by the measured quadrupole deformations, shown in Figs. 5d, 5e and 5f. It is noteworthy, that the observed $\beta_2\sim$0.25 for the decoupled bands in ^{130}Pr and ^{132}Pr lie between values of $\beta_2\sim$0.20, measured for the normally deformed structures, and those of $\beta_2\sim 0.30-0.35$ reported for the highly deformed bands which involve the $\nu i_{13/2}$ or the $\pi g_{9/2}$ orbital (see Table 1). Thus, the occupancy of the 1/2$^-$[541] ($f_{7/2}$,$h_{9/2}$) neutron orbital results in the observation of enhanced deformed bands for nuclei below $N = 73$. The corresponding growth in quadrupole deformation values, however, is not as large as those observed when the $\nu i_{13/2}$ or $\pi g_{9/2}$ orbital is occupied.

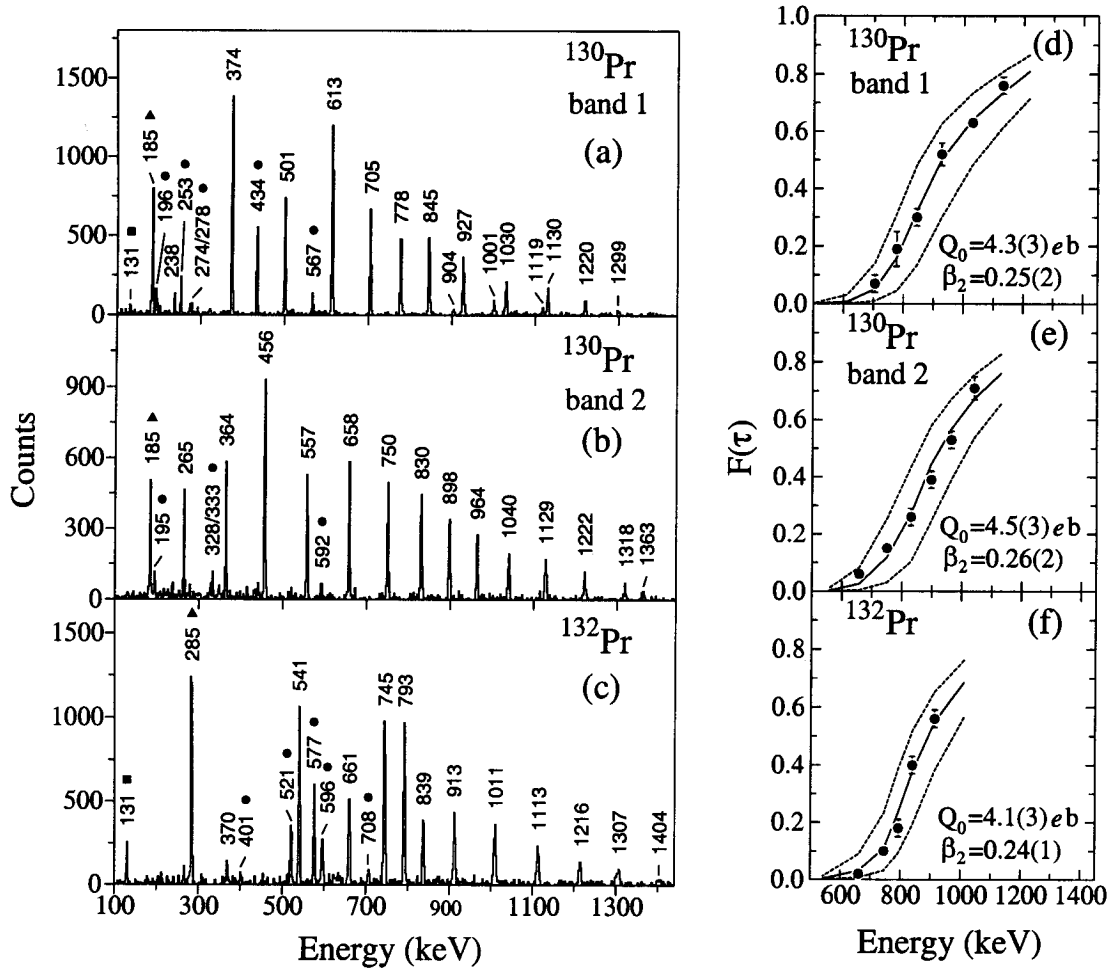

FIGURE 5. (a), (b) and (c) Doubly-gated coincidence γ-ray spectra from the thin target experiment for the decoupled bands in ^{130}Pr and ^{132}Pr. The peaks marked with circles correspond to inter-band transitions and those marked with triangles indicate transitions depopulating the $\pi h_{11/2}\otimes\nu h_{11/2}$ bands. The γ-rays labeled with squares are assigned as the $\pi h_{11/2}\otimes\nu h_{11/2}$ in-band transitions. (d), (e) and (f) The experimental (symbols) and calculated (solid and dashed lines) F(τ) values as a function of the γ-ray energy. The solid lines represent the best fit values and the deduced Q_0 and β_2 are indicated. The dashed curves correspond to values obtained with $Q_0\pm1$ *eb*.

SUMMARY AND OPEN PROBLEMS

The quadrupole moments of a number of bands, in several Nd and Pr nuclei, were measured using the Doppler-shift attenuation method as a part of our systematic study dedicated to understand the properties of highly deformed structures in mass~130 region. Differences in the observed deformations clearly demonstrate the important role played by the occupation of the $9/2^+[404]$ ($g_{9/2}$) proton, $1/2^+[660]$($i_{13/2}$) and $1/2^-[541]$ ($f_{7/2}$,$h_{9/2}$) neutron orbitals on the properties of the highly deformed bands.

These systematic data leave open several problems to be addressed by theory and further experiments.

(a) Due to differences in the experimental conditions, the parameterization of the stopping power data and the modeling of the sidefeeding lifetime contributions, the conclusive comparison between the quadrupole deformations reported by various authors is rather limited. The lack of experimental knowledge on the stopping powers is a difficult problem to overcome and direct measurements would be clearly valuable. Lifetime measurements, in the picosecond range, can be performed for in-band states using both the coincidence Recoil Distance Method, which is not sensitive to the stopping powers, and the DSAM lineshape technique. The comparison of the two sets of data could be used to extract useful information about the stopping powers. In addition, the improved efficiency of the new large detector arrays allows the reduction of some of the systematic pitfalls

inherent in the DSAM techniques, by measuring the properties of a large number of structures simultaneously, in a single experiment. It has been shown here, that if the time structure of the sidefeeding is not taken into account correctly, the extracted quadrupole deformations for highly deformed bands will be lower (usually ~10%) than the true values. One immediate approach that can be successfully applied in removing the effect of unknown sidefeeding is to gate on Doppler-shifted transitions at the top of the band of interest. It would also be valuable to perform quadrupole moment measurements as a function of spin using the DSAM lineshape analysis technique.

(b) The properties of the highly deformed bands are often judged only by the relative behavior of the dynamic moments of inertia, which depends not only on the variations in deformation, but also on the magnitude of the pairing field, which changes with the increase of both the seniority and rotational frequency, and the quasiparticle alignment effects. The deformation parameters of many structures in this mass region are successfully described by calculations which allow pairing correlations to take a full effect and also by those which completely ignore them, thus raising the question: "Is the pairing important and what role does it play?". The presence or absence of the pairing correlations will have also important consequences on the decay out mechanism of the highly deformed structures, as revealed for example in other mass regions.

(c) Some of the observed irregularities in collective bands at high spin are suggested to arise from a simple crossing between specific single-particle levels in a rotating frame. Such a scenario, however, may not be true in the case of odd-odd nuclei, as well as for high seniority bands in other nuclei, due to the additional effect of the residual nucleon-nucleon ($\pi-\nu$, $\pi-\pi$ and $\nu-\nu$) interactions. The role played by the residual interactions and their influence on the properties of the highly deformed structures clearly needs a further investigation. In the odd-odd nuclei there is a significant increase in the density of bands which results in greater fragmentation of the γ-ray intensity flow and consequently in lower population of a particular structure. In addition, there are difficulties and complications in linking together observed structures, particularly where low-energy transitions and/or long lifetimes are presented, which result in tentative spin and parity assignments, thus generating much speculations about the involved configurations. Many more highly deformed bands, formed by the coupling of different proton (neutron) orbitals to the deformation driving $\nu i_{13/2}$ or $\nu(f_{7/2},h_{9/2})$ neutron ($g_{9/2}$ proton), are expected in odd-odd nuclei in this mass region. The observation of these structures and the elucidation of their detailed properties remain a challenge for further studies.

ACKNOWLEDGMENTS

The authors wish to extend their thanks to the staff of the LBNL GAMMASPHERE facility and the crew of the 88″ Cyclotron for their assistance during these experiments. The software support of D.C. Radford and H.Q. Jin is greatly appreciated. Discussions with L.L. Riedinger are gratefully acknowledged. Support for this work was provided by the U.S. Department of Energy under Contract No. DE–AC03–765F00098 and Grant No. DE–FG02–88ER40406, the National Science Foundation, the State of Florida and the U.K. Engineering and Physical Sciences Research Council. MAR and JS acknowledge the receipt of a NATO Collaborative Research Grant.

REFERENCES

1. Wyss, R., *et al.*, *Phys. Lett.* **B215**, 211–217 (1988).
2. Galindo-Uribarri, A., *et al.*, *Phys. Rev.* **C50**, R2655–R2659 (1994).
3. Galindo-Uribarri, A., *et al.*, *Phys. Rev.* **C54**, 1057–1069 (1996).
4. Galindo-Uribarri, A., *et al.*, *Phys. Rev.* **C54**, R454–R458 (1996).
5. Wadsworth, R., *et al.*, *Nucl. Phys.* **A526**, 188–204 (1991).
6. Janssens, R., and Stephens, F., *Nucl. Phys. News* **6**, 9–17 (1996).
7. Sarantites, D.G., *et al.*, *Nucl. Instrum. Methods Phys. Res.* **A381**, 418–432 (1996).
8. Alexander, T.K., and Forster, J.S., *Advances in Nuclear Physics*, New York: Plenum Press, 1978, vol.10, pp.197.
9. Radford, D.C., *Nucl. Instrum. Methods Phys. Res.* **A361**, 297–305 (1995).
10. Moore, E.F., *et al.*, *Phys. Rev.* **C55**, R2150–R2154 (1997).
11. Ziegler, J.F., Biersack, J.P., and Littmark, U., *The Stopping and Range of Ions in Solids*, New York: Pergamon Press, 1985; Ziegler, J.F., (private communication).
12. Blaugrund, A.E., *Nucl. Phys.* **88**, 501–512 (1966).
13. Mullins, S.M., *et al.*, *Phys. Rev* **C45**, 2683–2692 (1992).

14. Medina, N.H., *et al.*, *Nucl. Phys.* **A589**, 106–116 (1995).
15. Diamond, R.M., *et al.*, *Phys. Rev.* **C41**, R1327–R1331 (1990).
16. Petrache, C.M., *et al.*, *Phys. Rev.* **C57**, R10–R14 (1998).
17. Wadsworth, R., *et al.*, *J. Phys. G: Nucl. Phys.* **13**, L207–L212 (1987).
18. Beck, E.M., *et al.*, *Phys. Rev. Lett.* **58**, 2182–2185 (1987).
19. Bazzacco, D., *et al.*, *Phys. Lett.* **B309**, 235–240 (1993).
20. Bazzacco, D., *et al.*, *Phys. Rev.* **C49**, R2281–2284 (1994).
21. Deleplanque, M.A., *et al.*, *Phys. Rev.* **C52**, R2302–2305 (1995).
22. Lunardi, S., *et al.*, *Phys. Rev.* **C52**, R6–R10 (1995).
23. Petrache, C.M., *et al.*, *Nucl. Phys.* **A617**, 228–248 (1997).
24. Petrache, C.M., *et al.*, *Phys. Lett.* **B219**, 145–150 (1996).
25. Wilssau, P., *et al.*, *Phys. Rev.* **C48**, R494–497 (1993).
26. Clark, R.M., *et al.*, *Phys. Rev. Lett.* **76**, 3510–3513 (1996).
27. Regan, P.H., *et al.*, *J. Phys. G: Nucl. Phys.* **18**, 847–858 (1992).
28. Afanasjev, A.V., and Ragnarsson, I., *Nucl. Phys.* **A608**, 176–201 (1996).
29. Brown, T.B., *et al.*, *Phys. Rev.* **C56**, R1210–R1214 (1997).
30. Kondev, F.G., *et al.*, *Eur. Phys. J.* **A2**, 249–251 (1998).
31. Smith, B.H., *et al.* (to be published); Riedinger, L.L., *et al.* (private communication).
32. Hauschild, K., *et al.*, *Phys. Rev.* **C50**, 707–715 (1994).
33. Shi, S., *et al.*, *Phys. Rev.* **C37**, 1478–1484 (1988).
34. Petrache, C.M., *et al.*, *Nucl. Phys.* **A635**, 361–383 (1998).
35. Ma, R., *et al.*, *Phys. Rev.* **C37**, 1926–1931 (1988).